A faster numerical scheme for a coupled system to model soil erosion and suspended sediment transport

Minh-Hoang Le, Stéphane Cordier, Carine Lucas, Olivier Cerdan

▶ **To cite this version:**

Minh-Hoang Le, Stéphane Cordier, Carine Lucas, Olivier Cerdan. A faster numerical scheme for a coupled system to model soil erosion and suspended sediment transport. 2014. hal-00957667v1

HAL Id: hal-00957667

https://hal.science/hal-00957667v1

Preprint submitted on 10 Mar 2014 (v1), last revised 19 Jan 2015 (v2)

HAL is a multi-disciplinary open access archive for the deposit and dissemination of scientific research documents, whether they are published or not. The documents may come from teaching and research institutions in France or abroad, or from public or private research centers.

L'archive ouverte pluridisciplinaire **HAL**, est destinée au dépôt et à la diffusion de documents scientifiques de niveau recherche, publiés ou non, émanant des établissements d'enseignement et de recherche français ou étrangers, des laboratoires publics ou privés.

A faster numerical scheme for a coupled system to model soil erosion and suspended sediment transport

M.-H. Le[1-2], S. Cordier[1], C. Lucas[1] and O. Cerdan[2]

[1]Univ. Orléans, CNRS, MAPMO, UMR 7349, Fédération Denis Poisson, F-45067, Orléans, France
[2]BRGM, Risks Department, 3 rue Claude Guillemin, 45060 Orléans, France

Abstract

Overland flow and soil erosion play an essential role in water quality and soil degradation. Such processes, involving the interactions between water flow, suspended particles and soil, are classically described by a well-established system of PDE coupling the shallow water equations and the Hairsine-Rose model. The numerical approximation of this coupled system requires advanced methods to preserve some important physical and mathematical properties in particular the steady states, the positivity of both water depth and sediment concentrations. Recently, a well-balanced MUSCL-Hancock scheme has been proposed by Heng et al. [25] in which an additional and artificial limitation on the time step is required to ensure the positivity of sediment concentrations. This artificial condition can lead the computation to be costly when dealing with very shallow flow and wet/dry fronts. The main result of this paper is to propose a new and faster scheme for which only the CFL condition of shallow water equations is sufficient to preserve the positivity of sediment concentrations. In addition, the use of up-to-date numerical methods allows to obtain easily a well-balanced scheme, to guarantee the positivity of water depth and to verify the maximum principle for sediment concentrations in the convective step. The numerical scheme is tested on classical benchmarks, and we also perform a test on a realistic topography to justify again the quality of proposed approach.

Keywords: shallow water equations, finite volume method, well-balanced scheme, numerical stability, positivity, CFL conditon, Hairsine-Rose model, soil erosion.

Introduction

Soil erosion is a complex phenomenon affected by many factors such as climate, topography, soil characteristics, vegetation and anthropogenic activities such as cultivation practices (see e.g. [12]). Soil erosion and sediment transport can have adverse effects on the stormwater quality [37]. Erosion process due to rainfall and overland flow can be described in three stages: detachment, transport and deposition of soil particles. The detachment occurs when the flow shear stress or the kinetic energy of raindrop exceeds the cohesive strength of the soil particles. Once detached, the particles can be transported downstream as non-cohesive sediments before their deposition [32].

Water flow induces sediment transport and changes in the surface morphology. The sediments carried by the water flow can be transported either along the bed as bedload in the form of sliding and rolling grains, or in suspension as suspended load advected by the main flow. Bedload particles are located in a few grain diameters thick layer situated on the soil and the velocities of these particles are smaller than the flow velocity. At the opposite, the suspended particles are transported at the velocity of the flow. In practice, suspended load usually comprises finer fractions that are more controlled by supply than energy.

It is possible to discriminate between bedload and suspension of transport by using the Rouse number (see e.g. [30]). But the threshold can be different depending on the experiment, see [29, 33].

The erodibility of a soil depends on the particle size distribution and in particular it is well known that the sedimentation is a size-selective process [19]. In the context of erosion with suspension transport, Hairsine and Rose [21, 22] developed a soil erosion model, called HR model hereafter, taking into account the particle's size distribution and their impacts in the process of erosion and sediment transport. Moreover, the detachment-entrainment of the original soil, the redetachment-reentrainment of deposited sediments and the deposition are considered as concurrent processes. It also models the development of the deposited layer that differs from the original soil in its cohesion and particle size distribution.

The present work concerns to numerical simulation of overland flow including soil erosion. Recently, Heng et al. [25] proposed an appropriate numerical method for the coupled system combining shallow water (SW) equations and HR model. Numerical tests showed that this scheme performs well in terms of accuracy and robustness for both the water and sediment transport. Moreover, this scheme is the unique well-balanced method developed for this coupled model up to our knowledge, unlike the case of SW equations where many advanced solvers can be found in literature. Later, Heng et al. [26] applied their implementation to a series of detailed flume-scale experiments to test the model's ability to reproduce the observed data including the dynamic evolution of the sediment-size distribution.

A remarkable limit of the solver proposed in [25] is that in addition to the Courant-Friedrichs-Lewy (CFL) condition of SW equations, an another *artificial* restriction on the time step must be verified to ensure the non-negativity of sediment concentration. In particular, the authors stated that this restriction can lead the computation to be costly when dealing with very shallow flow and wet/dry fronts. This problem is the motivation of our work where we found a more efficient (and faster) scheme being able to relax the mentioned restriction.

The outline of the paper is as follows: in section 1, the system of governing equations considered in Heng et al. [25] is firstly generalized into two-dimension case. For the sake of completeness, the HR equations are also recalled using the same notations with [25, 26]. In section 2, we propose a new approach for which only the CFL condition of SW equations is sufficient to ensure the positivity of water depth and sediment concentration. Next, we validate the implementation of the new method in section 3 with some benchmark tests selected in the literature. We justify by a two-dimensional test on a realistic topography the quality of proposed scheme in term of performance: for overall of simulation, the simulation is at least 100 time faster thank to the proposed improvement.

1 Complete system, coupling hydrodynamic, erosion and sediment transport

In this section, we recall the equations we use in the following, expressing the conservation principle of both water height and sediments (see [21, 22] for example). They consist in a system coupling the two-dimensional SW equations with the HR model for I classes of sediments, namely

$$\begin{cases} \partial_t h + \nabla \cdot (h\mathbf{u}) = R - I_r, \\ \partial_t (h\mathbf{u}) + \nabla \cdot (h\mathbf{u} \otimes \mathbf{u}) + \nabla \left(\dfrac{gh^2}{2} \right) = -gh(\nabla z_b + S_f), \\ \partial_t (c_i h) + \nabla \cdot (c_i h\mathbf{u}) = e_i + e_{ri} + r_i + r_{ri} - d_i, \\ \partial_t m_i = d_i - e_{ri} - r_{ri}, \\ \partial_t z_b = -\dfrac{1}{(1-\phi)\rho_s} \displaystyle\sum_{i=1}^{I} (e_i + e_{ri} + r_i + r_{ri} - d_i), \end{cases} \tag{1}$$

(for $i = 1, \ldots, I$), where the $(2I + 3)$ unknowns of system are

- h the water depth (m),
- $\mathbf{u} = (u, v)$ the horizontal velocity of the flow (m/s),
- z_b the bed surface elevation (m),
- c_i the sediment concentration in mass of i-th class (kg/m^3),
- m_i their mass in the deposited layer (kg/m^2).

Note that the transport rate of suspended sediment was assumed to be lower than a turbidity threshold, so it has no contribution in the momentum of the water flow. In other words, the sediment is considered as a passive pollutant in the flow. This hypothesis is not too restrictive for the applications since the concentration in volume of sediment is often less than 10%.

Let us recall the source terms of SW equations: the water source terms are R and I_r representing the rainfall intensity and the infiltration rate respectively (m/s). For the friction slope S_f, two formulations are usually chosen in hydrological models: the Manning friction law $S_f = \mathbf{n}^2\mathbf{u}|\mathbf{u}|/h^{4/3}$ or the Darcy-Weisbach law $S_f = f\mathbf{u}|\mathbf{u}|/(8gh)$. In this work, the Manning friction coefficient n and the Darcy-Weisbach coefficient f are regarded as constants.

The HR model describes the erosion processes of I particle-size classes, as illustrated in Fig. 1. For the

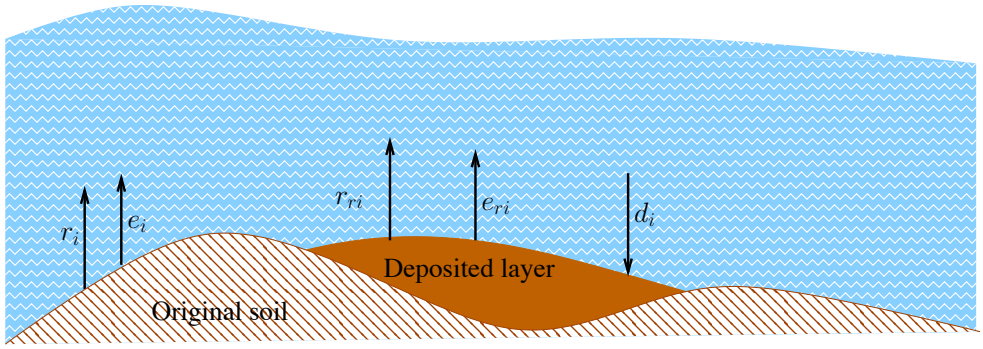

Figure 1: Processes interacting between the original soil, deposited layer and suspended sediments in overland flow.

i-th class, we denote by v_{fi} the settling velocity (m/s), e_i and r_i the rates of rainsplash detachment and flow entrainment from the original soil respectively, e_{ri} and r_{ri} the rates of rainsplash re-detachment and flow re-entrainment from the deposited layer respectively and finally d_i the sedimentation rate (kg/(m^{2}s)). These source terms are given by the HR equations:

$$e_i = (1 - H)p_i a R, \tag{2}$$

$$e_{ri} = H\frac{m_i}{m_T} a_d R, \tag{3}$$

$$r_i = (1 - H)p_i \frac{F(\omega - \omega_{cr})}{J}, \tag{4}$$

$$r_{ri} = H\frac{m_i}{m_T}\frac{F(\omega - \omega_{cr})}{\frac{\rho_s - \rho_w}{\rho_s} gh}, \tag{5}$$

$$d_i = c_i v_{fi}, \tag{6}$$

where a and a_d are the detachability coefficients of the original soil and the deposited layer respectively, ρ_w and ρ_s the densities of water and sediment respectively, and p_i the fraction of i-th class in the original soil.

As soil erosion due to flow is a threshold process, the stream power $\omega = \rho_w g h |S_f||\mathbf{u}|$ must exceed the critical value ω_{cr} to entrain soil particles. In such a situation, we denote by F the effective fraction of excess stream power in entrainment and re-entrainment, and J the energy expended in entraining a unit mass of cohesive sediment. Once the deposited layer has been created, it protects the original soil and consequently reduces the rate of detachment and entrainment of the original soil. To characterise this effect, we define $H = \min\{1, m_T/m_T^*\}$ the fractional shielding of the original soil by the deposited layer, with $m_T = \sum_{i=1}^{I} m_i$ the accumulated mass per unit area of deposited layer and m_T^* the required mass of deposited layer to shield completely the original soil.

Since the raindrop energy is reduced as it penetrates the surface water layer, the soil detachability coefficients a, a_d and the critical mass m_T^* are decreasing functions of the water depth h. In [26], a power law proposed by Proffitt et al. [36] was used to describe this depending:

$$\begin{pmatrix} a \\ a_d \\ m_T^* \end{pmatrix} = \begin{pmatrix} a_0 \\ a_{d0} \\ m_{T0}^* \end{pmatrix} \times \begin{cases} 1 & \text{if } h \leq h_0 \\ (h_0/h)^b & \text{if } h > h_0 \end{cases} \tag{7}$$

where a_0, a_{d0} and m_{T0}^* are the related maximum values at the breakpoint depth h_0, which is about 0.33 mean drop diameter and b is an exponent in the range of 0.66 ± 0.07.

Finally, ϕ represents the porosity of eroded bed and g the gravity acceleration.

In the next section, we explain how to numerically discretize equations (1)–(6), paying attention to preserve physical properties such as non-negativity of the water height and the sediment concentration.

2 Numerical method

The numerical method presented here is a finite volume approach, as in [25], but the treatment of the equations differs. More precisely, the convection of sediments by the flow is computed thanks to an upwind scheme, the homogeneous flux for the SW equations is not the same, and the erosion-sedimentation source terms are split in two parts, instead of using an explicit discretization.

Finite volume schemes are known to be robust for numerical simulation of conservative systems since this method ensures the conservation by construction. In the present works, structured grids have been chosen for spatial discretization of the domain because on the one hand, digital topographic maps are often provided on such meshes, and on the other hand, the extension of an existing one-dimensional numerical scheme to the two-dimensional case is straightforward. For the sake of simplicity, we only describe hereafter the numerical method for one-dimensional system.

Introducing the conservative variables $\mathbf{U} = (h, hu, c_1 h, \ldots, c_I h)$, $\mathbf{V} = (m_1, \ldots, m_I, z_b)$, the one-dimensional system of governing equations writes:

$$\begin{cases} \partial_t \mathbf{U} + \partial_x F(\mathbf{U}) = S_0 + S_1, \\ \partial_t \mathbf{V} = S_2, \end{cases} \tag{8}$$

where the flux and the source terms are given by

$$F(\mathbf{U}) = \begin{pmatrix} hu \\ hu^2 + gh^2/2 \\ c_1 hu \\ \vdots \\ c_I hu \end{pmatrix}, \quad S_0 = \begin{pmatrix} 0 \\ -gh\partial_x z_b \\ 0 \\ \vdots \\ 0 \end{pmatrix},$$

$$S_1 = \begin{pmatrix} R - I_r \\ -ghS_f \\ e_1 + e_{r1} + r_1 + r_{r1} - d_1 \\ \vdots \\ e_I + e_{rI} + r_I + r_{rI} - d_I \end{pmatrix}, \quad S_2 = \begin{pmatrix} d_1 - e_{r1} - r_{r1} \\ \vdots \\ d_I - e_{rI} - r_{rI} \\ -\frac{\sum_{i=1}^{I}(e_i + e_{ri} + r_i + r_{ri} - d_i)}{(1-\phi)\rho_s} \end{pmatrix}.$$

Let us explain in what follows the main steps of the algorithm. First of all, remark that the topographical source term S_0 contains the derivative in space corresponding to the bottom slope while S_1 and S_2 are cell-centered terms related to water source terms, bed friction, erosion and sedimentation. For this reason, S_0 needs to be discretized together with the flux $F(\mathbf{U})$. On the contrary, S_1 and S_2 can be treated in a separate step by a system of ODE, without adding numerical oscillations. In other words, we adopt a time-splitting strategy that first solves the following hyperbolic system with source term S_0 (called convective step)

$$\partial_t \mathbf{U} + \partial_x F(\mathbf{U}) = S_0, \tag{9}$$

and then corrects the computed value by taking into account the source terms S_1 and S_2 via the system

$$\begin{cases} \partial_t \mathbf{U} = S_1, \\ \partial_t \mathbf{V} = S_2. \end{cases} \tag{10}$$

Note that the second order in time can be reached repeating these two steps with Heun's method, *i.e.* the second order Runge-Kutta TVD scheme. In what follows, we detail the numerical scheme for equations (9)–(10), at the second order in space but first order in time.

2.1 Convective step

The convective step corresponds to the resolution of system (9). We notice that the I transport equations of sediment concentrations have the same formula. For the sake of compactness, we shorten the considered system replacing the last I equations by a generic one, using c instead of c_i to denote the concentration of the considered sediment-size class. Then, the compacted system writes

$$\partial_t h + \partial_x(hu) = 0, \tag{11}$$

$$\partial_t(hu) + \partial_x(hu^2 + gh^2/2) = -gh\partial_x z_b, \tag{12}$$

$$\partial_t(ch) + \partial_x(chu) = 0. \tag{13}$$

Starting from a given value $\mathbf{U}^n$, the variables obtained after this step are denoted with a bar: $\overline{h}, \overline{hu}, \overline{ch}$.

2.1.1 Numerical scheme for the shallow water equations

This numerical scheme aims at solving the well-known SW equations (11)–(12). It has been recently implemented in FullSWOF software. We only recall its main ideas, as it is not the central part of this article. For more details, we refer the reader to [17].

The well-balanced numerical scheme reads

$$\begin{aligned}\overline{U}_j &= \begin{pmatrix}\overline{h}_j\\ \overline{hu}_j\end{pmatrix} = U_j^n - \frac{\Delta t}{\Delta x}\left(F^n_{j+1/2L} - F^n_{j-1/2R} - Fc^n_j\right) \\ &= U_j^n - \frac{\Delta t}{\Delta x}\left(\mathcal{F}\left(U^n_{j+1/2L}, U^n_{j+1/2R}\right) + S_{j+1/2L} - \mathcal{F}\left(U^n_{j-1/2L}, U^n_{j-1/2R}\right) - S_{j-1/2R} - Fc^n_j\right),\end{aligned} \tag{14}$$

where $\Delta x, \Delta t$ are the space and time steps respectively, j the current cell index and n the time iteration, $\mathcal{F}$ is the numerical flux for the homogeneous SW equations, $S_\bullet$ source terms due to the topography, and Fc_j an additional centered term that preserves consistency and well-balancing. Note that the source terms $S_\bullet$ and Fc_j do not contribute to the first component. In the computations of the values at the interfaces $U^n_{j\pm1/2L,R}$, the numerical scheme (14) includes a linear reconstruction (we consider the MUSCL reconstruction, see [46]) and the hydrostatic reconstruction (see [3] and recall the limitation for large bottom slopes and small water depth given in [15]).

For the homogeneous flux $\mathcal{F}$, any consistent numerical flux can be chosen, such as Godunov, Rusanov, HLL, Roe, or the ones obtained by the kinetic or relaxation methods. Note that Heng et al. [25] used a Roe type solver; however, a remarkable drawback is that, in certain situations, it can produce negative depths which are obviously physically incorrect, and usually crashes the execution of the program. In particular for applications where the flow is very shallow in parts of the domain, or in fact becomes dry in regions, the Roe solver is almost certain to produce negative depths. In this work, we adopted the HLL flux [24] which is known to be a simple and efficient solver for both accuracy and implementation aspects. An appropriate choice for the wave speed estimates can lead the HLL Riemann solver to satisfy automatically an entropy inequality, to resolve isolated shocks exactly, and to preserve positivity. When both sides of the cell interface are wet, a natural choice is to compare the maximum and minimum characteristics velocities evaluated at of both left and right given states. These estimates can also be improved using the Roe average, see [6]. For the wet/dry transitions, a more suitable estimation for the wave speeds can be derived using the exact Riemann solution [45]. Consequently, the resulting scheme preserves the positivity and is well adapted to wet/dry transitions[1].

2.1.2 A new approach for the sediment transport

A first important remark is that, in equation (13), the suspended sediments are simply convected by the flow. At the numerical level, contrarily to Heng et al. [25], we choose an upwind scheme to solve this equation, that is

$$\overline{(ch)}_j = (ch)^n_j - \frac{\Delta t}{\Delta x}\left(F^{ch}_{j+1/2} - F^{ch}_{j-1/2}\right). \tag{15}$$

The related upwind flux $F^{ch}_{j+1/2}$ for sediment transport is given by

$$F^{ch}_{j+1/2} = \begin{cases} c^n_j F^h_{j+1/2} & \text{if } F^h_{j+1/2} = \left(\mathcal{F}\left(U^n_{j+1/2L}, U^n_{j+1/2R}\right)\right)_1 > 0, \\ c^n_{j+1} F^h_{j+1/2} & \text{else,}\end{cases} \tag{16}$$

in which $\mathcal{F}$ is the homogeneous numerical flux and $(\bullet)_1$ stands for the first component. In fact, combining (16) with HLL flux (for SW equations) is equivalent to use a HLLC solver [45].

One must also note that this numerical scheme for the sediment transport does not bring any condition on the time step: in the complete convection step (14)–(15), the CFL condition is only related to the wave speeds s_L, s_R of the SW equations

$$\frac{\Delta t}{\Delta x}\max\{|s_L|, |s_R|\} \le C, \text{ with } \begin{cases} C = 1 \text{ at the first order,} \\ C = 0.5 \text{ at the second order.}\end{cases} \tag{17}$$

[1]The detailed method have been implemented in FullSWOF_2D, see https://sourcesup.renater.fr/projects/fullswof-2d/

Let us recall that, under the positivity assumption on the water depth, which is guarantees by section 2.1.1, the scheme (15) with the upwind flux (16) is consistent with equation (13) and preserves the positivity of the sediment concentration, *i.e.* $c \geq 0$. Moreover, the discrete form of the maximum principle is also verified, *i.e.*

$$\overline{c}_j \leq \max(c_{j-1}^n, c_j^n, c_{j+1}^n), \quad \forall\ j, n.$$

A detail proof of these properties can be found in [9].

2.1.3 Numerical treatment of boundary condition

The Riemann invariants of SW equations are used to compute the water depth and the flow velocity on the ghost cells (see [11] and [17]). For the sediments, we can compute the sediment concentration at the ghost cells thanks to definition (16) of the upwind flux F^{ch}. For example at upstream with transmissible or reflexive boundary types, we set the value at the left ghost cell 0: $c_0^n = c_1^n$. For the case of an imposed sediment flux q_s, we set the value at the left ghost cell 0: $c_0^n = q_s / F_{1/2}^h$.

2.2 Source terms discretization

At the end of the convective step, we obtain the state $\overline{\mathbf{U}}$ from the given value $\mathbf{U}^n$ via the well-balanced scheme (14) and the upwind scheme (15). The next step is to compute $(\mathbf{U}, \mathbf{V})^{n+1}$ from $(\overline{\mathbf{U}}, \mathbf{V}^n)$ by solving the system of ODE (10). We apply an Euler type scheme performed on each cell to compute the new state at time t^{n+1}. We omit the cell index j to simplify the expressions of the scheme.

The water source and friction terms are treated as usual, see [17]. The rain and the infiltration terms are treated explicitly as they involve no particular numerical difficulties such as steady-state or stability preservations. The infiltration rate can be handled using any of the approximate methods available such as Green-Ampt [20], Philip [35], and Horton [28] or a more exact method based on a solution to Richards equation [39]. In this work, we will use the Green-Ampt model. See [4, 13, 18, 38] for more in-depth discussions on the choice of the parameters of the model. Concerning the friction terms, we adopt a semi-implicit discretization (as in [11, 31, 17]) to preserve the stability when simulations involve wet/dry evolving fronts, and to keep the well-balanced property obtained in the convective step.

Let us turn to the main difficulty brought by the source terms: the contributions of erosion and sedimentation given by system (10). This system expressing the HR model for I sediment classes can be rewritten as the following equations, for $i = 1, \ldots, I$:

$$\partial_t(c_i h) = e_i + e_{ri} + r_i + r_{ri} - d_i, \tag{18}$$

$$\partial_t m_i + \partial_t(c_i h) = e_i + r_i, \tag{19}$$

$$\rho_s(1-\phi)\partial_t z_b + \sum_{i=1}^{I} \partial_t(c_i h) = 0. \tag{20}$$

System (18)–(20) can be computed directly by using an explicit Euler's method. Nevertheless, it requires a special treatment for each situation called *before-ponding* and *after-ponding* that correspond to two different behaviors of erosion processes. These cases are differentiated numerically by a small artificial threshold h_p of the water depth.

In the following, we first recall the method proposed in [25, 26]; in the second part, we introduce a new treatment of theses equations, enabling us to keep the CFL condition of SW equations.

2.2.1 Classical approach for erosion and sedimentation, modifying the CFL condition

We detail here how equations (18)–(20) have been discretized, depending on the erosion process.

Before-ponding. When $h \leq h_p$, the detached sediments are not transported but accumulate into the deposited layer on the soil surface. Equations (18)–(20) reduce to $\partial_t m_i = e_i$. This situation is treated numerically, as mentioned in [26], by setting

$$\begin{aligned} &(c_i h)^{n+1} = 0, \\ &(m_i)^{n+1} = (m_i)^n + \overline{(c_i h)} + \Delta t (e_i)^n. \end{aligned} \tag{21}$$

After-ponding. When $h > h_p$, the detached sediments can be suspended in flow. Physically, the amount of sediment deposited over a time increment cannot be greater than that in the flow. In other words, a negative value of $c_i h$ does not make sense. While the positivity of sediment concentration is well preserved in convective step, this is no longer evident when using an explicit approximation to solve equations (18)–(20). That is the reason why, in [25], another restriction on the time step has been introduced, namely

$$\Delta t \leq \left(\frac{c_i h}{d_i} \right)^n = \frac{h^n}{v_{fi}}, \quad \text{for } i = 1, \ldots, I. \tag{22}$$

The authors found that for small water depths, the time step Δt is governed by this condition rather than by the CFL condition (17) of SW equations.

2.2.2 A new approach for erosion and sedimentation, with an unchanged CFL condition

We notice that the previous restriction is caused by the use of the explicit discretization for equation (18). To overcome this problem, we can solve numerically this equation by two steps consisting successively in (i) the phase of sedimentation and (ii) the phase of erosion

$$\begin{aligned} &(i) \quad \partial_t (c_i h) = -d_i = -\frac{v_{fi}}{h} (c_i h), \\ &(ii) \quad \partial_t (c_i h) = e_i + e_{ri} + r_i + r_{ri}. \end{aligned}$$

Since the water depth remains constant in these steps, the advantage of this splitting is that the first equation can be solved using an analytic solution while an explicit discretization can be used for the second one. The resulting scheme for equation (18) writes

$$\begin{aligned} &\overline{\overline{(c_i h)}} = \exp\left\{ -\frac{v_{fi}}{\overline{h}} \Delta t \right\} \overline{(c_i h)}, \\ &(c_i h)^{n+1} = \overline{\overline{(c_i h)}} + \Delta t (e_i + r_i)^n + \Delta t (e_{ri} + r_{ri})^n. \end{aligned} \tag{23}$$

Another remark at numerical level is that while $(e_i + r_i)^n$ can be computed directly from equations (2), (4), the quantity $\Delta t \sum_{i=1}^{I} (e_{ri} + r_{ri})^n$ may not be greater than $(m_T)^n$. Indeed $\Delta t \sum_{i=1}^{I} (e_{ri} + r_{ri})^n$ is the quantity of sediment available for re-detachment and re-entrainment. From equations (3) and (5), we define $(e_r + r_r)^n$ at each time t^n as the total capacity of re-detachment and re-entrainment from the deposited layer

$$(e_r + r_r)^n = H \left(a_d R + \frac{F(\omega - \omega_{cr})}{\frac{\rho_s - \rho_w}{\rho_s}} \right).$$

Hence the total rate of re-detachment and re-entrainment of the sediment size class i is given by

$$\Delta t (e_{ri} + r_{ri})^n = \frac{(m_i)^n}{(m_T)^n} \min \left\{ (m_T)^n, \Delta t (e_r + r_r)^n \right\}. \tag{24}$$

The scheme (23) together with (24) shows that $(c_i h)^{n+1} \geq 0$ since $\overline{(c_i h)} \geq 0$ (obtained from the upwind scheme (15)). The positivity of c_i is thus preserved without requiring the supplementary condition (22) on the time step.

Using (23), we can now solve, in a conservative way, equations (19)–(20) to obtain the mass of deposited layer and the topography at time t^{n+1}

$$\begin{aligned}(m_i)^{n+1} &= (m_i)^n + \Delta t(e_i + r_i)^n - \left((c_i h)^{n+1} - \overline{(c_i h)}\right), \\ (z_b)^{n+1} &= (z_b)^n - \frac{1}{\rho_s(1-\phi)} \sum_{i=1}^{I} \left((c_i h)^{n+1} - \overline{(c_i h)}\right).\end{aligned} \tag{25}$$

Let us sum up the main properties of proposed method. The numerical scheme combining (14)–(15), (23), (25) is conservative, well-balance, positivity preserving for both of the water depth and the sediment concentration. In particular, only the CFL condition of SW equations is required to ensure the stability of the overall numerical scheme.

3 Numerical results

As explained before, the erosion model we consider is a coupling between the SW equations and the HR model. We thus used a SW code, to which we added an erosion component. For the SW part, we used the C++ code *FullSWOF* (Full Shallow Water equations for Overland Flow). This software, developed in the framework of the multi-disciplinary project METHODE ANR-07-BLAN-0232, is distributed under CeCILL-V2 (GPL compatible) free software license, and available at http://www.univ-orleans.fr/mapmo/soft/FullSWOF/, see [17]. The resolution of the SW equations can be performed at second order in time and space using the MUSCL reconstruction and the hydrostatic reconstruction, as noticed in the previous section.

In this section, we present numerical validations of the proposed approximation for system (1) coupling SW equations to the HR model, using equations (14)–(15), (23), (25). Unfortunately, there is no time and space-depending analytic solution available for this system. So we validate separately the convective part, modelling overland flow and suspended sediment, and the HR model describing the processes of erosion and sedimentation. As the convective step has been developed on the basis of *FullSWOF*, we do not need to perform again the numerical validations for the hydrodynamic part, *i.e.* SW equations, discretized with equation (14) (see [16, 17] for various benchmarks tested on *FullSWOF*). After this series of tests for the validation of the numerical method, we give a two-dimensional example on a real topography for which we compare the time step of our new approach to the time step that must be used if we follow Heng et al. [25] approach. We also show that the computed quantities (water height, concentrations) stay non-negative.

3.1 Tests on the convective step for the sediment transport

In order to test the new part of the convective step (equation (15)), it is necessary to cancel the erosion and sedimentation processes to impose $S_1 = S_2 = 0$; for this, it is sufficient to set $S_f = a = a_d = v_f = 0$.

We want to test two important properties of this numerical scheme computing the evolution of sediment concentration in shallow flow: the consistency and the preservation of equilibria. Thus we run two tests proposed in [2] where a finite volume with kinetic interpretation is used to simulate the transport of a passive pollutant by the flow.

3.1.1 Dam break on a flat bottom with sediments

This classical test simulate the case of a dam break on a flat bottom with no friction, in which the concentration of sediment is different on each side of the dam. In other words, the configuration of this test is exactly the Riemann problem of the homogeneous system of (11, 12, 13). We consider a spatial domain of length 2000 m, discretized by an uniform mesh with 100 cells, and we set the final time of

simulation to $T = 240$ s. The dam is located at the center of the domain, that is at $x_0 = 1000$ m. For the initial conditions, we set

$$\begin{cases} h_l = 1. \\ q_l = 0. \\ c_l = 0.7 \end{cases} \quad \text{on the left boundary, and} \quad \begin{cases} h_r = 0.5 \\ q_r = 0. \\ c_r = 0.5 \end{cases} \quad \text{on the right boundary.}$$

The interest of this test is that we have an expression of the exact solution (see [43]). From left to right, the solution is separated by two constant intermediate states. The first intermediate state connects to the left given state by a rarefaction wave propagating with a speed $u - \sqrt{gh}$. The second intermediate state connects to the right given state by a shock wave propagating with a speed $u + \sqrt{gh}$. These intermediate states are separated by a discontinuity wave propagating with the flow speed. Recall that in the exact solution the values of h and u do not change across the contact waves in the intermediate region, while the concentration c transported with the flow does not change across the non-linear waves but changes, discontinuously, across the contact wave. To check the convergence property of the proposed method, we performed this test with the first and second order schemes.

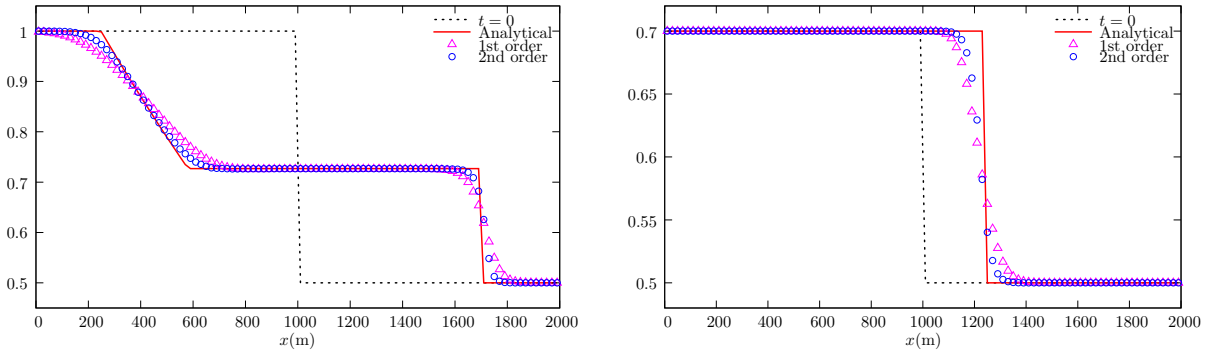

(a) Water depth

(b) Sediment concentration

Figure 2: Dam break: numerical results at $T = 240$s.

In Fig. 2, we plotted the initial condition (dotted line), the analytic solution (continuous line), the first order approximation (triangles) and the second order approximation (circles) for the water depth and the sediment concentration. The numerical results show that the analytic solution is approximated well and that the second order is, as expected, a better approximation than the first order.

3.1.2 Preservation of the steady state of the lake at rest

Next we want to verify numerically the steady state of the lake at rest. In this case, the equilibrium of the concentration must be also preserved. So we use a non-flat bottom

$$z_b(x) = \begin{cases} 0 & \text{if } 0 \le x < 8, \\ 0.2 - 0.05(x - 10)^2 & \text{if } 8 \le x \le 12, \\ 0 & \text{if } 12 < x \le 20 \end{cases}$$

discretized by a uniform mesh with 100 cells. The initial condition is

$$h(0, x) + z_b(x) = 1, \quad q(0, x) = 0, \quad \text{and} \quad c(0, x) = \begin{cases} 0 & \text{if } 0 \le x < 8, \\ 1 & \text{if } 8 \le x \le 10, \\ 0 & \text{if } 10 < x \le 20. \end{cases}$$

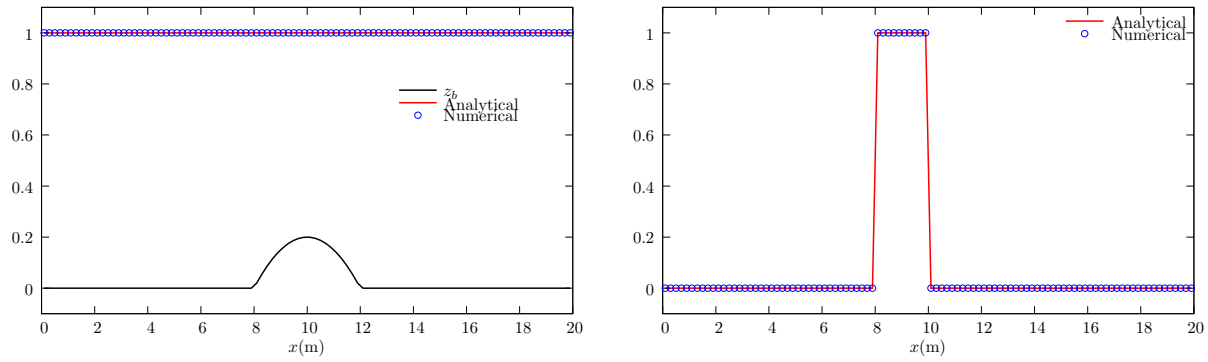

(a) Free surface elevation

(b) Sediment concentration

Figure 3: Lake at rest.

Note that the initial condition satisfies the equilibrium, which means that we test wether the code is able to preserve the steady state.

In the exact solution, the initial state is preserved and it is analytically proved that the upwind scheme (15) maintains this property (see [9]). We present in Fig. 3 the numerical results after 100 s, for the free surface elevation and the sediment concentration. In both results, the stationary solution is preserved exactly.

3.2 Tests with some specific solutions of HR model

After numerical tests presented on the convective step, let us check the functionality of the erosion and sedimentation step, approximated by schemes (23)–(25). In the literature, some analytic, semi-analytic or numerical solutions are available for the HR model with specific assumptions (see [41, 42, 23, 27, 40, 5]). Here, we compare our numerical results with two reference solutions proposed by Sander et al. [42] and Hogarth et al. [27] as these solutions have shown a good agreement with experiments.

3.2.1 A steady state analytic solution: net deposition in overland flow

In this section, we are interested in a special configuration called net deposition region. It is the zone where the sediment flux decreases downslope and the deposited layer develops very rapidly to completely shield the original soil (so the shielding factor is $H \approx 1$). We also assume that the water flow is deep enough (greater than 3 drop diameters), allowing us to neglect the re-detachment process by rainfall. Indeed the impact of raindrops in that case is largely absorbed by the water layer. Hence the re-entrainment and deposition are the only active erosion mechanisms. The equations of mass conservation of sediment reduce to

$$\partial_t(c_i h) + \partial_x(c_i q) = r_{ri} - d_i, \tag{26}$$

$$\partial_t m_i = d_i - r_{ri}. \tag{27}$$

Hairsine et al. [23] presented a steady state single-class analytic solution when there is no rainfall and a constant flow rate imposed at the top of slope, *i.e.* $q = q_0 = cst$. Sander et al. [42] extended the solution

to the case of multi-size classes. Their solution writes

$$\begin{aligned} c_i(x) &= c_{i0}\left(\frac{c_I(x)}{c_{I0}}\right)^{\frac{v_{fi}}{v_{fI}}}, \quad \text{for } i = 1, 2, \ldots, I-1, \\ m_i(t,x) &= v_{fi}c_i(x)\left(1 - \frac{\gamma^*}{\sum_{i=1}^{I} v_{fi}c_i(x)}\right)t, \quad \text{for } i = 1, 2, \ldots, I, \end{aligned} \tag{28}$$

where c_{i0} is the concentration of the sediment size class i at upstream and

$$\gamma^* = \gamma q_0^{2/5}\left(1 - \frac{q_{cr}}{q_0}\right), \quad \gamma = \frac{F\rho_s\rho_w S_0 K^{3/5}}{\rho_s - \rho_w}, \text{ with } K = \frac{\sqrt{S_0}}{\mathbf{n}}, \quad q_{cr} = \frac{\omega_{cr}}{\rho_w g S_0}.$$

Finally, the concentration $c_I(x)$ of the last sediment size class can be computed analytically by solving the following equation

$$\frac{dc_I(x)}{dx} = \left(\frac{\gamma^*}{\sum_{i=1}^{I} v_{fi}c_{i0}\left(\frac{c_I}{c_{I0}}\right)^{\frac{v_{fi}}{v_{fI}}}} - 1\right)\frac{v_{fI}c_I}{q_0}$$

which leads to

$$\int_{c_{I0}}^{c_I(x)} \left(\frac{\gamma^*}{\sum_{i=1}^{I} v_{fi}c_{i0}\left(\frac{\overline{c}_I}{c_{I0}}\right)^{\frac{v_{fi}}{v_{fI}}}} - 1\right)^{-1} \frac{d\overline{c}_I}{\overline{c}_I} = \frac{v_{fI}}{q_0}x. \tag{29}$$

We perform this benchmark with the parameters used in [25]:

- $S_0 = 0.02,\ \mathbf{n} = 0.01,\ q_0 = 0.00125$ m^2/s, $\rho_s = 2600$ kg/m^3;
- the settling velocity (in mm/s) of 10 sediment classes of a soil in the loam belt of central Belgium are taken from experiments data of Beuselinck et al. [8]: 0.00043, 0.0037, 0.02, 0.083, 0.23, 0.46, 0.74, 1.1, 1.7, and 3.2 respectively;
- we set $c_{i0} = 10$ kg/m^3 at the boundary and use $F = 0.01,\ \omega_{cr} = 0.186$ W/m^2;
- the initial condition is given by $c_i(0, x) = 10,$ for $i = 1, \ldots, I$.

Fig. 4 presents the numerical results with $\Delta t = 0.05$s and 100 cells, at time $T = 10$ min, in order to reach the steady state. More precisely, the sediment concentrations for the classes numbered 1, 4, 7, 9 and 10 are plotted as functions of the space variable. One can note that the numerical and analytic results are similar.

3.2.2 A transitory solution: rainfall-driven erosion

This benchmark is a case where the solution is time-dependent. However, there is no such analytic solutions available in literature for the coupled system of SW equations and the HR equations. The solution proposed by Hogarth et al. [27] is derived from the system coupling the kinematic wave model [47] and the HR equations.

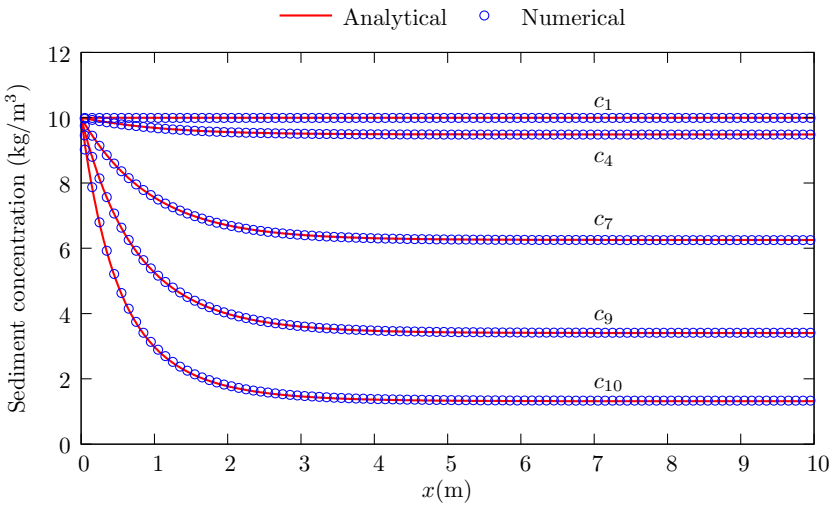

Figure 4: Net deposition in overland flow.

A solution for the kinematic wave approximation. This numerical solution of rainfall-driven erosion was proposed to predict the dynamics of sediment eroded by rainfall impacts when there is no inflow of water at the top of the eroded slope, and no infiltration of water in the soil. This solution allows to investigate changes with time, downslope distance and settling velocity of the concentration of eroding sediment. Contrary to the previous test, the flow-driven processes are not present in the configuration of this benchmark and the rainfall impact is the only erosion agent. The mass conservation equations of HR model reduce to

$$\partial_t(c_i h) + \partial_x(c_i q) = e_i + e_{ri} - d_i, \tag{30}$$
$$\partial_t m_i = d_i - e_{ri}. \tag{31}$$

Considering a stationary solution of kinematic model with no inflow, and assuming that in the original soil, each class contains an equal mass of sediment, *i.e.* $p_i = 1/I$. A numerical solution was computed by using a semi-implicit upwinding finite difference method which lead to the following scheme after rearranging

$$\begin{aligned}(c_i)_j^{n+1} = &\left(1 - \frac{\lambda q}{h} - \frac{\kappa}{h}\left(1 + \frac{v_{fi}}{R}\right)\right)(c_i)_j^n + \frac{\lambda q}{h}(c_i)_{j-1}^n \\ &+ \frac{\kappa}{h}\left(\beta(m_i)_j^{n+1} + \frac{a}{I}\left(1 - \frac{\sum_{i=1}^{I}(m_i)_j^{n+1}}{m_T^*}\right)\right),\end{aligned} \tag{32}$$
$$(m_i)_j^{n+1} = (1 - \kappa\beta)(m_i)_j^n + \frac{\kappa v_{fi}}{R}(c_i)_j^n.$$

where $\lambda = \Delta t/\Delta x$, $\kappa = R\Delta t$ and $\beta = a_d/m_T^*$. An initial condition (at $t = 0$) and a boundary condition (at the upstream $x = 0$) for each sediment class are required to close the scheme (32)

$$\begin{aligned} \text{initial condition:} \quad & (c_i)_j^0 = 0, \quad (m_i)_j^0 = 0, \\ \text{boundary condition:} \quad & (c_i)_0^n = 0, \quad (m_i)_0^n = 0, \end{aligned} \qquad \text{for } i = 1, \ldots, I.$$

Numerical results. Finally, we perform this last benchmark with the parameters used in [25]:

- domain setting: $L = 5.8$ m discretized by 100 cells, $\Delta t = 0.002$ s;

- for the hydraulic part: $S_0 = 0.004,\ \mathbf{n} = 0.06,\ R = 100$ mm/h;
- about the sediment types, we consider 10 classes with settling velocities (in mm/s) 0.21, 0.71, 3.3, 10.9, 19.4, 31.2, 69.1, 139, 210, and 300 respectively;
- for erosion parameters, we set $a = 920$ kg/m^3, $a_d = 14190$ kg/m^3, $m_T^* = 0.0767$ kg/m^2.

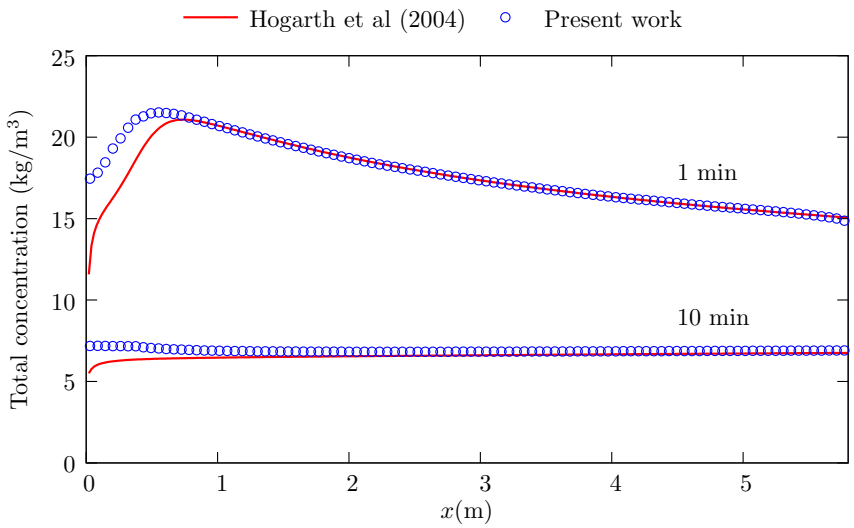

Figure 5: Rainfall-driven erosion.

On Fig. 5 we plotted, for two different times, the variations in space of the total sediment concentration obtained by our new method, coupling the SW and HR equations, and the approximation of the analytic solution of the kinematic wave coupled with HR model, given by equation (32). We find again a good agreement between the two solutions, the difference on the left part of the domain lying in the difference between the SW and the kinematic wave models. We also obtain good results compared to experiment observations of Proffitt et al. [36]: sediment concentration decreases with time until the steady-state concentration is reached.

3.3 A two dimensional case test

The previous one dimensional tests using analytic solutions justify the important properties of proposed method such as convergence and steady state preserving. Before entering into our last experiment, it is important to keep in mind that the present objective is not to validate the physical model (8) considered in this paper. In fact, this topic has been investigated in several publications, and moreover Heng et al. [26] presented an in-depth discussion of the model parameters. This case test aims to check the good performance of the proposed solver and to emphasize the overall quality of this new approach.

We perform a two dimensional simulation with a realistic irregular topography taking into account the erosion and deposition effects. The chosen configuration includes wet/dry fonts, water infiltration and rainfall-driven erosion process with multiple sediment size class. Moreover, we will pay attention on the gain in computational time only governing by (17) thank to the larger time stepping allowed of proposed scheme.

This simulation used data collected on the plot of Thies (Senegal) realized by IRD [44] in the project PNRH RIDES. The dataset is freely available at http://www.umr-lisah.fr/Thies_2004/. The plot was 10 m long by 4 m wide, with a 1% slope, and sandy soil (1% clay, 7% silt, 43% fine sand, 49% coarse

sand). The surface was raked in order to form a slight V shape, with 1% slope longitudinally and 1% slope towards the median axis of the plot. The purpose of the V shape was to avoid rill development at the edge of the plot. A 2-hour long rainfall was applied at a constant intensity of 70 mm/h in order to maintain steady runoff and infiltration rate. See [34] for more detail on experiment design. The granulometry of the sandy soil is given in Table 1 and the related settling velocities of 10 sediment classes are calculated using Cheng's formula [14].

Grain size (μm)	10	20	50	100	150	200	250	500	750	1000
Portion (%)	1	2	4	13	15	14	13	32	5	1
Settling velocity (mm/s)	0.04	0.16	1	3.8	7.8	12.6	17.8	43.1	64.6	82.1

Table 1: Granulometry of the sandy soil.

On initial condition and model parameters, the plot surface was dry at the beginning of simulation while the sandy soil was considered as completely cohesion. This consists to set $h^0 = c_i^0 = m_i^0 = 0,\ \forall i = 1, \cdots, 10$. The friction was calculated by Darcy-Weisbach's formula while the infiltration rate was given by Green-Ampt model. Detail on the used parameters can be found in [17]. For each grain size d_s, we set an associated ponding depth $h_p = 1.5 d_s$. By regarding the range of grain size in table 1, this setting allows to simulate simultaneously the *before-* and *after-ponding* situation between the different sediment classes in particular during transition period. We used $\rho_w = 1000$, $\rho_s = 2000$, and according to the discussion in [26], others parameters of the HR model, i.e. those in equations (2-7), are chosen as: $F = 0.1$, $\omega_{cr} = 0.1525$, $J = 100$, $h_0 = 0.66 \times 10^{-3}$, $b = 1$, $a_0 = 150$, $a_{d0} = 1500$ and $m^*_{T0} = 1$.

The simulation result at the end of rainfall even ($t = 120$ mm) is given by Fig. 6. First, we see that except at the main flow localising in the rill, the flow at all most of other regions in the plot are very shallow ($h \sim 1$mm) or rather dry (fig. 6a). Moreover, the water flux (fig 6b) is nearly negligible except at the outlet, so the stream power is unlikely to exceed its critical value ($\omega_{cr} = 0.1525$ was calculated from Abrahams et al. [1]'s formula). This means that the flow has no contribution into sediment entrainment but just caries the detached particles. Consequently, the phenomenon which happened in the plot is typically rainfall-driven erosion. This conclusion can be justified again by regarding fig. 6c which visualizes the mass of deposited layer. In major region of the plot, rainfall detachment accumulates soil particles into non-cohesive (deposited) layer and the related critical value was rapidly reached. Recall that the soil was initially cohesive. In the main flow where the thickness of water layer is sufficient important, i.e. $h \gg h_0$ in equation (7), the rainfall erosivity is limited since the raindrop energy is reduced as it penetrates the surface water layer.

Fig. 6d,e,f expresses the size-selectivity characteristic of suspended flow. Recall that the grain size distribution was initially uniform in space and given by table 1. As the flow is very shallow, we pay a particular attention on the fine grains ($d_s \leq 100\mu$m), for example silt and fine-sand. Fig. 6d-e show that the first class in grain size ($d_s \leq 10\mu$m) contributes a major portion in suspended while it was initially only 1% in original soil. On the contrary, the 4th sediment class ($d_s \leq 10\mu$m) is nearly absent in the main flow and oppositely with their significant portion (13%) in original soil (fig. 6f).

Finally, it is important to check the main interest of proposed scheme by regarding the gain in computational efficiency. Recall that our method only requires the CFL condition of SW equations while the additional condition of HR equations must be verified in the works of Heng et al. [25]. For this propose, we compare the maximum allowed timestep given by (17) et (22). Moreover, it is useful to recall that condition (22) can be relaxed slightly, as proposed in [26], by only applying it on the wet region of the plot where the detached particles can be transported in suspension ($h > h_p$). This allows to avoid the fact that $\Delta t \to 0$ during pre-ponding period. Fig. 7 presents the maximum allowed timesteps given by (17) et (22) which allows to justify the quality of proposed approach. Firstly, during transition period (first 10 minutes of rainfall event), the timestep of HR equation is very restrictive contrary to what happens for SW equations. Next, when the flow reaches steady state, the timestep of SW equations is in order of $10^{-2}s$ and two orders of magnitude more than that of HR equation ($10^{-4}s$). Consequently for overall of

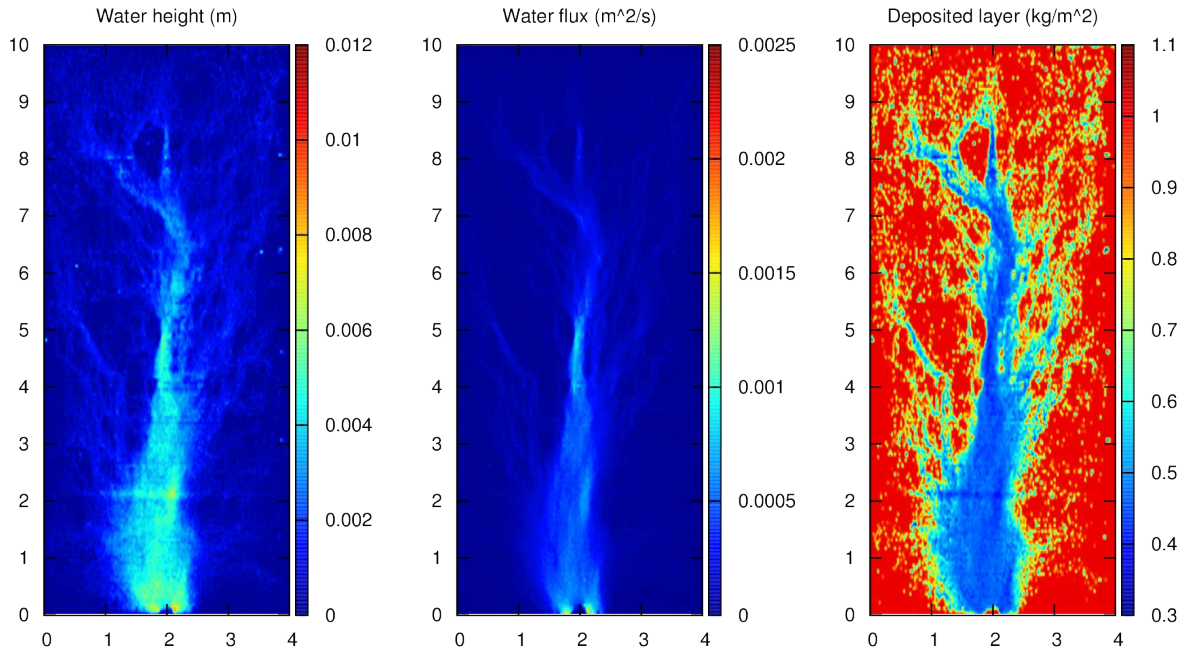

(a) (b) (c)

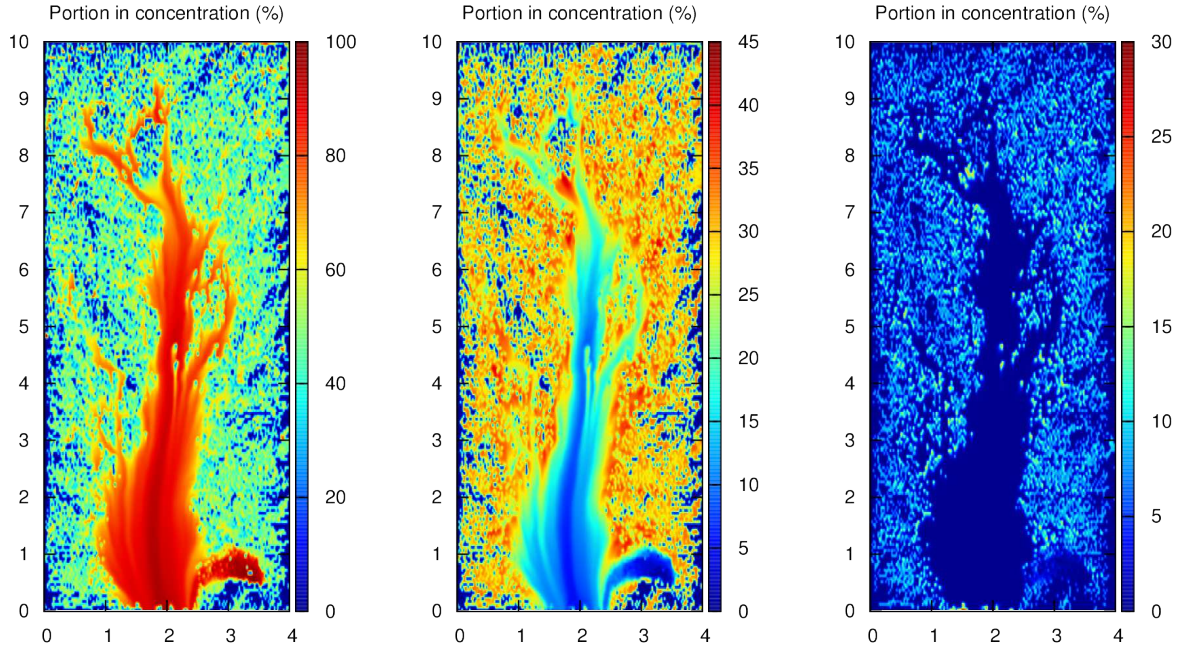

(d) $d_s = 10\mu$m (e) $d_s = 20\mu$m (f) $d_s = 100\mu$m

Figure 6: Simulation result at $t = 120$ minutes

simulation, the condition (22) is at least 100 time more restrictive than (17). It is important to recall a well-known numerical effect which states that more the timestep is reduced, more numerical diffusion is added.

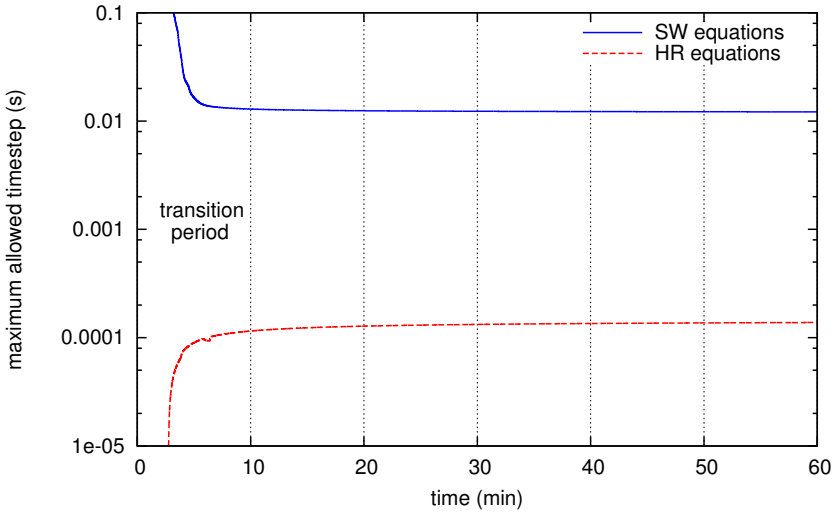

Figure 7: Gain in performance by using large timestep

Conclusions

The system coupling SW equations with HR model allows to simulate complex scenarios of soil erosion by rainfall and overland flow on a non-uniform topography. This model predicts not only the topographical evolution and the eroded sediment flux but also the particle-selectivity during erosion processes. We have constructed an alternative numerical solver, based on the hydrostatic reconstruction, with some advanced properties compared to the well-balanced scheme proposed recently by Heng et al. [25]. It has been shown that the present method preserves important physical and mathematical properties of the system as it is well-balanced and positivity preserving. An additional advantage of the presented scheme is that it requires only the CFL condition associated to SW equations to ensure the stability of numerical solution and consequently offers a more efficient solution.

In term of modularity and robustness, the proposed approximation of the erosion part is less depending on the numerical approximation of the hydrodynamic part. Indeed, only the numerical flux of water $F^h_{j+1/2}$ is required to compute the flux of sediments $F^{ch}_{j+1/2}$ *via* equation (16). In other words, the numerical method presented in this paper can be adapted to any well-balanced and positivity preserving approximation for SW equations. Over the last few years, other advanced solvers for SW equations have been proposed, e.g. those presented in [10, 7]; a natural extension of this work will be to investigate the coupling with these recently proposed solvers. Finally in each timestep, the computation corresponding to each sediment class, i.e. equation (23), is independently each others and thus can be performed by the way parallel (for exemple with OpenMPI). This property becomes interesting when we deal with an important number of sediment class.

Acknowledgements. The authors would like to thanks Frédéric Darboux for the numerous discussions and his comments and suggestions, and the ANR VMCS program BIOCRUST for its financial support.

References

[1] Athol D. Abrahams, Gary Li, Chitra Krishnan, and Joseph F. Atkinson. Predicting sediment transport by interrill overland flow on rough surfaces. *Earth Surface Processes and Landforms*, 23(12):1087–1099, 1998. ISSN 1096-9837. doi: 10.1002/(SICI)1096-9837(199812)23:12⟨1087::AID-ESP934⟩3.0.CO;2-4. URL http://dx.doi.org/10.1002/(SICI)1096-9837(199812)23:12<1087::AID-ESP934>3.0.CO;2-4.

[2] E. Audusse and M.-O. Bristeau. Transport of pollutant in shallow water: A two time steps kinetic method. *M2AN*, 37(2):389–416, March 2003. doi: 10.1051/m2an:2003034. URL http://dx.doi.org/10.1051/m2an:2003034.

[3] E. Audusse, F. Bouchut, M.-O. Bristeau, R. Klein, and B. Perthame. A fast and stable well-balanced scheme with hydrostatic reconstruction for shallow water flows. *SIAM J. Sci. Comput.*, 25(6):2050–2065, 2004. doi: 10.1137/S1064827503431090.

[4] D.A. Barry, J.-Y. Parlange, L. Li, D.-S. Jeng, and M. Crapper. Green–Ampt approximations. *Advances in Water Resources*, 28(10):1003–1009, 2005. ISSN 0309-1708. doi: 10.1016/j.advwatres.2005.03.010. URL http://www.sciencedirect.com/science/article/B6VCF-4G4N0GR-2/2/03d464d73ad9d57a6587ab3b80a94e5f.

[5] D.A. Barry, G.C. Sander, S. Jomaa, B.C.P. Heng, J.-Y. Parlange, I.G. Lisle, and W.L. Hogarth. Exact solutions of the Hairsine–Rose precipitation-driven erosion model for a uniform grain-sized soil. *Journal of Hydrology*, 389(34):399–405, 2010. ISSN 0022-1694. doi: 10.1016/j.jhydrol.2010.06.016. URL http://www.sciencedirect.com/science/article/pii/S0022169410003513.

[6] P. Batten, N. Clarke, C. Lambert, and D. M. Causon. On the choice of wavespeeds for the HLLC Riemann solver. *SIAM J. Sci. Comput.*, 18(6):1553–1570, November 1997. ISSN 1064-8275. doi: 10.1137/S1064827593260140. URL http://dx.doi.org/10.1137/S1064827593260140.

[7] C. Berthon and F. Foucher. Efficient well-balanced hydrostatic upwind schemes for shallow-water equations. *Journal of Computational Physics*, 231(15):4993–5015, 2012. ISSN 0021-9991. doi: 10.1016/j.jcp.2012.02.031. URL http://www.sciencedirect.com/science/article/pii/S0021999112001453.

[8] L. Beuselinck, G. Govers, A. Steegen, and T. A. Quine. Sediment transport by overland flow over an area of net deposition. *Hydrological Processes*, 13(17):2769–2782, 1999. ISSN 1099-1085. doi: 10.1002/(SICI)1099-1085(19991215)13:17⟨2769::AID-HYP898⟩3.0.CO;2-X. URL http://dx.doi.org/10.1002/(SICI)1099-1085(19991215)13:17<2769::AID-HYP898>3.0.CO;2-X.

[9] F. Bouchut. *Nonlinear stability of finite volume methods for hyperbolic conservation laws, and well-balanced schemes for sources*, volume 2/2004. Birkhäuser Basel, 2004. doi: 10.1007/b95203.

[10] F. Bouchut and T. de Luna. A subsonic-well-balanced reconstruction scheme for shallow water flows. *SIAM Journal on Numerical Analysis*, 48(5):1733–1758, 2010. doi: 10.1137/090758416. URL http://epubs.siam.org/doi/abs/10.1137/090758416.

[11] M.-O. Bristeau and B. Coussin. Boundary conditions for the shallow water equations solved by kinetic schemes. Technical Report 4282, INRIA, October 2001.

[12] O. Cerdan, G. Govers, Y. Le Bissonnais, K. Van Oost, J. Poesen, N. Saby, A. Gobin, A. Vacca, J. Quinton, K. Auerswald, A. Klik, F.J.P.M. Kwaad, D. Raclot, I. Ionita, J. Rejman, S. Rousseva, T. Muxart, M.J. Roxo, and T. Dostal. The rate and spatial distribution of soil erosion in Europe: A study based on erosion plot data. *Geomorphology*, 122:167–177, 2010. doi: 10.1016/j.geomorph.2010.06.011. URL http://www.sciencedirect.com/science/article/pii/S0169555X10002813.

[13] L. Chen and M.H. Young. Green-Ampt infiltration model for sloping surfaces. *Water Resources Research*, 42(7):1–9, 2006. ISSN 1944-7973. doi: 10.1029/2005WR004468. URL http://dx.doi.org/10.1029/2005WR004468.

[14] N.S. Cheng. Simplified settling velocity formula for sediment particle. *J. Hydraul. Eng*, 123(2): 149–152, 1997.

[15] O. Delestre, S. Cordier, F. Darboux, and F. James. A limitation of the hydrostatic reconstruction technique for shallow water equations. *Comptes Rendus Mathematique*, 350(13–14):677–681, 2012. ISSN 1631-073X. doi: 10.1016/j.crma.2012.08.004. URL http://www.sciencedirect.com/science/article/pii/S1631073X12002245.

[16] O. Delestre, C. Lucas, P.-A. Ksinant, F. Darboux, C. Laguerre, T.-N.-T. Vo, F. James, and S. Cordier. SWASHES: a compilation of Shallow Water Analytic solutions for Hydraulic and Environmental Studies. *International Journal for Numerical Methods in Fluids*, 72(3):269–300, 2013. ISSN 1097-0363. doi: 10.1002/fld.3741. URL http://dx.doi.org/10.1002/fld.3741.

[17] O. Delestre, F. Darboux, F. James, C. Lucas, C. Laguerre, and S. Cordier. FullSWOF: A free software package for the simulation of shallow water flows. Submitted, 2014. URL http://hal.archives-ouvertes.fr/hal-00932234.

[18] M. Esteves, X. Faucher, S. Galle, and M. Vauclin. Overland flow and infiltration modelling for small plots during unsteady rain : numerical results versus observed values. *Journal of Hydrology*, 228: 265–282, 2000.

[19] A. Farenhorst and R.B. Bryan. Particle size distribution of sediment transported by shallow flow. *CATENA*, 25(1–4):47 – 62, 1995. ISSN 0341-8162. doi: 10.1016/0341-8162(94)00041-C. URL http://www.sciencedirect.com/science/article/pii/034181629400041C.

[20] W.H. Green and G.A. Ampt. Studies on soil physics. *The Journal of Agricultural Science*, 4:1–24, 1911.

[21] P.B. Hairsine and C.W. Rose. Rainfall detachment and deposition: Sediment transport in the absence of flow-driven processes. *Soil Sci. Soc. Am. J.*, 55(2):320–324, 1991.

[22] P.B. Hairsine and C.W. Rose. Modeling water erosion due to overland flow using physical principles. II: rill flow. *Water Resources Research*, 28:245–250, 1992.

[23] P.B. Hairsine, L. Beuselinck, and G.C. Sander. Sediment transport through an area of net deposition. *Water Resources Research*, 38(6):22–1–22–7, 2002. ISSN 1944-7973. doi: 10.1029/2001WR000265. URL http://dx.doi.org/10.1029/2001WR000265.

[24] A. Harten, P.D. Lax, and B. van Leer. On upstream differencing and Godunov-type schemes for hyperbolic conservation laws. *SIAM Review*, 25(1):35–61, January 1983.

[25] B.C.P. Heng, G.C. Sander, and C.F. Scott. Modeling overland flow and soil erosion on nonuniform hillslopes: A finite volume scheme. *Water Resources Research*, 45(5):W05423, 2009. ISSN 1944-7973. doi: 10.1029/2008WR007502. URL http://dx.doi.org/10.1029/2008WR007502.

[26] B.C.P. Heng, G.C. Sander, A. Armstrong, J.N. Quinton, J.H. Chandler, and C.F. Scott. Modeling the dynamics of soil erosion and size-selective sediment transport over nonuniform topography in flume-scale experiments. *Water Resour. Res.*, 47(2):W02513, February 2011. ISSN 0043-1397. URL http://dx.doi.org/10.1029/2010WR009375.

[27] W.L. Hogarth, J.-Y. Parlange, C.W. Rose, G.C. Sander, T.S. Steenhuis, and A. Barry. Soil erosion due to rainfall impact with inflow: an analytical solution with spatial and temporal effects. *Journal of Hydrology*, 295(1-4):140–148, 2004. ISSN 0022-1694. doi: 10.1016/j.

jhydrol.2004.03.007. URL http://www.sciencedirect.com/science/article/B6V6C-4CTBF67-2/2/a4478d5399a4abad930963ec74ba0b92.

[28] R.E. Horton. The role of infiltration in the hydrologic cycle. *Trans. Am. Geophys. Union*, 14:446–460, 1933.

[29] P.-Y. Julien. *Erosion and sedimentation*. Cambridge University Press, 280pp, 1998.

[30] J. P. Le Roux. Grains in motion: A review. *Sedimentary Geology*, 178(3-4):285–313, July 2005. doi: 10.1016/j.sedgeo.2005.05.009. URL http://dx.doi.org/10.1016/j.sedgeo.2005.05.009.

[31] Q. Liang and F. Marche. Numerical resolution of well-balanced shallow water equations with complex source terms. *Advances in Water Resources*, 32(6):873–884, 2009. ISSN 0309-1708. doi: 10.1016/j.advwatres.2009.02.010. URL http://www.sciencedirect.com/science/article/B6VCF-4VR9FHT-3/2/5218868dcfded7d34380666f23000855.

[32] W.S. Merritt, R.A. Letcher, and A.J. Jakeman. A review of erosion and sediment transport models. *Environm. Model. Software*, 18(8-9):761–799, 2003.

[33] G.H. Merten, M.A. Nearing, and A.L.O. Borges. Effect of sediment load on soil detachment and deposition in rills. *Soil Sci. Soc. Am. J.*, 65:861–868, 2001.

[34] C. Mügler, O. Planchon, J. Patin, S. Weill, N. Silvera, P. Richard, and E. Mouche. Comparison of roughness models to simulate overland flow and tracer transport experiments under simulated rainfall at plot scale. *Journal of Hydrology*, 402(12):25 – 40, 2011. ISSN 0022-1694. doi: http://dx.doi.org/10.1016/j.jhydrol.2011.02.032. URL http://www.sciencedirect.com/science/article/pii/S0022169411001648.

[35] J.R. Philip. The theory of infiltration: 1. the infiltration equation and its solution. *Soil Science*, 83: 345–357, 1957.

[36] A.P.B. Proffitt, C.W. Rose, and P.B. Hairsine. Rainfall detachment and deposition: experiments with low slopes and significant water depths. *Soil Sci. Soc. Am. J.*, 29:671–683, 1991.

[37] J.N. Quinton, G. Govers, K. Van Oost, and R.D. Bardgett. The impact of agricultural soil erosion on biogeochemical cycling. *Nature Geoscience*, 3:311–314, 2010. doi: 10.1038/ngeo838. URL http://www.nature.com/ngeo/journal/v3/n5/full/ngeo838.html.

[38] J.H. Richard. *Hydrology Handbook*. ASCE Manuals and Reports on Engineering Practice. American Society of Civil Engineers, 1996. ISBN 9780784401385.

[39] L.A. Richards. Capillary conduction of liquids through porous mediums. *Physics*, 1:318–333, November 1931.

[40] C.W. Rose, B. Yu, H. Ghadiri, H. Asadi, J.Y. Parlange, W.L. Hogarth, and J. Hussein. Dynamic erosion of soil in steady sheet flow. *Journal of Hydrology*, 333:449–458, 2007.

[41] G.C. Sander, P.B. Hairsine, C.W. Rose, D. Cassidy, J.-Y. Parlange, W.L. Hogarth, and I.G. Lisle. Unsteady soil erosion model, analytical solutions and comparison with experimental results. *Journal of Hydrology*, 178(1–4):351–367, 1996. ISSN 0022-1694. doi: 10.1016/0022-1694(95)02810-2. URL http://www.sciencedirect.com/science/article/pii/0022169495028102.

[42] G.C. Sander, P.B. Hairsine, L. Beuselinck, and G. Govers. Steady state sediment transport through an area of net deposition: Multisize class solutions. *Water Resources Research*, 38(6):23–1–23–8, 2002. ISSN 1944-7973. doi: 10.1029/2001WR000323. URL http://dx.doi.org/10.1029/2001WR000323.

[43] J. J. Stoker. *Water Waves: The Mathematical Theory with Applications*. Interscience Publishers, New York, USA, 1957.

[44] L. Tatard, O. Planchon, J. Wainwright, G. Nord, D. Favis-Mortlock, N. Silvera, O. Ribolzi, M. Esteves, and Chi-hua Huang. Measurement and modelling of high-resolution flow-velocity data under simulated rainfall on a low-slope sandy soil. *Journal of Hydrology*, 348(1-2):1–12, January 2008. doi: 10.1016/j.jhydrol.2007.07.016.

[45] E.F. Toro. *Shock-Capturing Methods for Free-Surface Shallow Flows*. Wiley and Sons Ltd., 2001.

[46] B. van Leer. Towards the ultimate conservative difference scheme. V. A second-order sequel to Godunov's method. *Journal of Computational Physics*, 32(1):101–136, 1979. ISSN 0021-9991. doi: DOI:10.1016/0021-9991(79)90145-1. URL http://www.sciencedirect.com/science/article/B6WHY-4DD1N8T-C5/2/9b051d1cfcff715a3d0f4b7b7b0397cc.

[47] D.A. Woolhiser and J.A. Liggett. Unsteady, one-dimensional flow over a plane–the rising hydrograph. *Water Resources Research*, 3(3):753–771, 1967.